Supplement of Atmos. Chem. Phys. Discuss., 15, 30017–30042, 2015
http://www.atmos-chem-phys-discuss.net/15/30017/2015/
doi:10.5194/acpd-15-30017-2015-supplement

Supplement of

Hydroxyl radicals from secondary organic aerosol decomposition in water

H. Tong et al.

Correspondence to: M. Shiraiwa (m.shiraiwa@mpic.de)

EPR experiments

The error bars in x-axis in Fig. 4 to 7 are based on uncertainties in SOA mass measurements in the balance. The same procedure was also applied to blank filters by immersing them into 10 mM BMPO and 0.5 mM Fe^{2+} ($FeSO_4 \cdot 7H_2O$, ≥ 99%, Sigma Aldrich) solutions, confirming that very little BMPO or iron residues would stick to filters upon extraction. Extractions and EPR measurements were conducted under dark conditions to avoid interferences due to photolysis. 16 ml glass vials with PTFE closure from VWR International GmbH were used. All the vials have been rinsed for 5-10 times with 10 mL fresh Milli-Q water each time and dried under ultrapure dry nitrogen gas (99.999%, Westfalen AG) before SOA extraction. Power free gloves (Carl Roth GmbH + Co.KG) and lab coat were used to avoid particles deposition from human body. Vials were used only once to avoid residue contaminations. Experiments were repeated with vials from different sets and there were no differences in the experimental results. In addition, the experimental results were fully consistent when the vials made from different materials (glass or polystyrene 15 ml conical tubes (VWR International GmbH)) were used. Particle concentrations in the laboratory were less than ~ 400 m^{-3} and we spent <3 s for opening and closing the vial caps to avoid contamination from deposition of particles into the samples. The filters were cleaned three times with 2-3 mL pure ethanol (ACS grade, VWR International S. A.S.) each time and dried with ultrapure dry nitrogen gas before SOA collection. The filter holder were cleaned with pure ethanol and Milli-Q water and dried with ultrapure dry nitrogen before experiment. OH radicals were not observed in different concentrations of hydrogen peroxide (TraceSELECT® Ultra, for ultratrace analysis) mixed with BMPO by an EPR. Thus, contaminations of transition metals during our handling procedure for particle extraction and analysis are negligible.

One example that includes the original and fitted spectra for BMPO/$^{\bullet}$OH adduct of β-pinene SOA and cumene hydroperoxide is shown in Fig. S1. The final root mean square deviation of the fitting was ~0.03, indicating a very good agreement between the experimental and simulated spectra. Five different radicals (BMPO-CH_3, t-BuO-BMPO, BMPO-OCH_3, and two isomers for BMPO-OH adduct) were found to coexist in tert-Butyl hydroperoxide solution. Good agreement between the fitted and measured spectrum confirms the dominance of OH radicals. The residual of the spectra can be regarded as trapped organic radicals.

Considering that the BMPO-OH adduct is stable over ~30 minutes, we have scanned samples over 50 times in ~20 min to elevate the signal to noise ratio of EPR spectra. The decay of DMPO-OH in water leads to uncertainty of ~11 % in quantification of trapped OH radicals. OH radicals in SOA water extracts were quantified using the spin counting method by removing interferences from organic radicals with the spin fitting method (see Methods and Fig. S1).

To investigate the role of water in the formation of OH radicals, ethanol (ACS grade, VWR International S. A.S.) was used as solvent. As shown in Fig. S5 c, BMPO-OH adducts were also observed in β-pinene SOA (E) and tert-Butyl hydroperoxide (F) in ethanol. These observations clearly show that OH radicals can be generated in the absence of water. Note that β-pinene SOA (Fig. 2B) and tert-Butyl hydroperoxide (Fig. 2G) yielded stronger OH signals in water compared to in ethanol. Additional experiments have shown that the OH formation efficiency of β-pinene SOA and tert-Butyl hydroperoxide in water increased by ~30% at 310 K compared to at a room temperature of 295 K. These results indicate that the source of OH radicals may be a combination of hydrolysis and thermal decomposition by organic hydroperoxides(Choe and Min, 2005).

Fig. S5 shows EPR spectra of mixtures of BMPO and cumene hydroperoxide (80%, Sigma Aldrich) with and without Fe^{2+}. The formation of OH and organic radicals upon decomposition of cumene hydroperoxide is clearly observed (A), which is substantially enhanced in the presence of Fe^{2+} due to Fenton-like reactions (B) (Chevallier., 2004). This is in agreement with previous observations of OH radicals generated by organic hydroperoxides in water (Guo et al., 2003). In contrast, no significant signals were observed for Di-tert-butyl peroxide solutions with and without

Fe^{2+} (Fig. S5). These observations suggest that the source of OH radicals is organic hydroperoxides (ROOH), but not organic peroxides (ROOR).

Kinetic Modelling

The modelling result is in agreement with the experimental observations of trapping OH with the BMPO spin trap shown in Fig. S2 for H_2O_2. The aqueous phase chemistry is dominated by the reaction between Fe^{2+} and H_2O_2 (R8) and subsequent trapping of OH by BMPO (R14). The predominant loss channel for the BMPO-OH adduct is oxidation by Fe^{3+} (R17). The same strategy is applied for modelling the dissociation of organic hydroperoxides (ROOH) in the absence and presence of Fe^{2+} in extracts of secondary organic aerosol (SOA). We assume that the reactions (1), (8), (10) and (12) for H_2O_2 also apply for ROOH as reactions (19) – (22). Additionally, thermal decomposition of ROOH is included, which dominates dissociation and hence OH production in the absence of Fe^{2+} (Fig. 4a). Reaction with organic molecules ("SOA") is a significant loss pathway for OH in our experiments. Since the initial concentration of BMPO was the same for all experiments, the ratio of SOA and BMPO varies between the different experiments. Hence, at higher SOA concentrations (Fig. 4a), a larger fraction of OH will react with organic molecules instead of BMPO, leading to the observed non-linear increase of the BMPO-OH signal. In the presence of Fe^{2+}, the Fenton-like reactions (19) and (20) lead to a much faster decomposition of ROOH. At higher Fe^{2+} concentrations however, the BMPO-OH adduct is effectively removed and the measured concentrations significantly reduced (Fig. 4b - d).

OH production rate in clouds and lung lining fluid

The OH production rate in cloud water due to Fenton reactions has been calculated. Typical dissolvable iron concentrations (Fe^{2+} and Fe^{3+} with a molar ratio of 1:1) and H_2O_2 concentrations in clouds ('Typical cloud' in Fig. 7a) were set to be 0.1 to 2.5 μM(Deguillaume et al., 2005) and 0.1 to 100 μM, respectively(Herrmann et al., 2015). A typical cloud water pH of 6 was assumed with a k_8 value of 1.1×10^{-18} cm^3 s^{-1} (Bataineh et al., 2012).

For estimation of the OH production rate in lung lining fluid by Fenton reactions, a typical iron concentration range of between 1 to 100 nM was used with Fe^{2+} to Fe^{3+} molar ratio of 1:1 (Hunter et al., 2013). It should be noted that there is a background concentration of iron within the LLF but this is not included during calculations as these iron ions are associated with ferritin and therefore unavailable for Fenton reactions (Ghio et al., 2006; Ghio, 2009). Additionally, typical H_2O_2 concentrations range of 0.001 to 1 μM in the LLF were chosen (Corradi et al., 2008). A pH value of 7 in the LLF (which is typical in healthy people (Paget-Brown et al., 2006)) was assumed and therefore k_8 in Table S1 would be expected to be 9.8×10^{-18} cm^3 s^{-1} (Bataineh et al., 2012), which lies within the range determined by global optimization.

In order to convert ambient concentration of SOA (μg m^{-3}) into an OH production rate in the LLF (P_{OH}, nM s^{-1}) the following equation was used: P_{OH} = (Ambient SOA concentration × breathing rate × PM deposition rate × R_{OH}) / total LLF volume, where ambient SOA concentrations ranged from 1 to 100 μg m^{-3}. R_{OH} is the OH formation efficiency of SOA in aqueous phase (Fig. 4). The breathing rate was assumed to be 230 cm^3 s^{-1}, the PM deposition rate was assumed to be 45% (Sarangapani and Wexler, 2000) and the total ELF volume was set to 25 ml (Walters, 2002).

Table S1. Equations and parameters used in the kinetic model.

Reaction number	Equation	Rate coefficient / $cm^3\ s^{-1}$	Reference
1	$H_2O_2 + OH \rightarrow H_2O + HO_2$	$k_1 = 5.5 \times 10^{-14}$	Christensen, et al.(Christensen et al., 1982)
2	$OH + OH \rightarrow H_2O_2$	$k_2 = 8.6 \times 10^{-12}$	Sehested, et al.(Sehested et al., 1968)
3	$OH + HO_2 \rightarrow H_2O + O_2$	$k_3 = 1.2 \times 10^{-11}$	Sehested, et al.(Sehested et al., 1968)
4	$HO_2 + HO_2 \rightarrow H_2O_2 + O_2$	$k_4 = 1.4 \times 10^{-15}$	Rush and Bielski(Rush and Bielski, 1985)
5	$H_2O_2 + HO_2 \rightarrow H_2O + O_2 + OH$	$k_5 = 5.0 \times 10^{-21}$	Koppenol et al. (1978)
6	$HO_2 + O_2^- \rightarrow H_2O_2 + OH^- + O_2$	$k_6 = 1.6 \times 10^{-13}$	Rush and Bielski(Rush and Bielski, 1985)
7	$H^+ + O_2^- \rightarrow HO_2$	$k_7 = 8.0 \times 10^{-11}$	Divišek and Kastening(Divišek and Kastening, 1975)
8	$Fe^{2+} + H_2O_2 \rightarrow Fe^{3+} + OH^- + OH$	$k_8 = 1.0 – 6.0 \times 10^{-17}$	
9	$Fe^{2+} + OH \rightarrow Fe^{3+} + OH^-$	$k_9 = 0.01 – 1.0 \times 10^{-11}$	Stuglik and Zagorski(Stuglik and PawełZagórski, 1981)
10	$Fe^{3+} + H_2O_2 \rightarrow Fe^{2+} + HO_2 + H^+$	$k_{10} < 1.0 \times 10^{-20}$	
11	$Fe^{3+} + HO_2 \rightarrow Fe^{2+} + O_2 + H^+$	$k_{11} = 3.3 \times 10^{-18}$	Rush and Bielski(Rush and Bielski, 1985)
12	$Fe^{2+} + H_2O_2 \rightarrow Fe^{4+}O^{2+} + H_2O$	$k_{12} = 0.5 - 8 \times 10^{-17}$	
13	$Fe^{4+} + Fe^{2+} \rightarrow 2Fe^{3+}$	$k_{13} = 10^{-19} – 10^{-16}$	
14	$BMPO + OH \rightarrow BMPO\text{-}OH$	$k_{14} = 0.06 - 6.0 \times 10^{-12}$	
15	$BMPO\text{-}OH \rightarrow Product$	$k_{15} = 0.1 - 2.0 \times 10^{-4}$	

16	BMPO-OH + Fe^{2+} → Product + Fe^{3+}	$k_{16} = 0.1 - 1.0 \times 10^{-19}$
17	BMPO-OH + Fe^{3+} → Product + Fe^{2+}	$k_{17} < 1.0 \times 10^{-20}$
18	BMPO-OH + Fe^{4+} → Product + Fe^{3+}	$k_{18} = 1 - 8.0 \times 10^{-18}$
19	Fe^{2+} + ROOH → Fe^{3+} + RO^{-} + OH	$k_{19} = k_8$
20	Fe^{2+} + ROOH → Fe^{3+} + RO + OH^{-}	$k_{20} < 1.0 \times 10^{-20}$
21	Fe^{3+} + ROOH → Fe^{2+} + RO_2 + H^{+}	$k_{21} = k_{10}$
22	OH + ROOH → ROH + HO_2	$k_{22} = k_1$
23	ROOH → RO + OH	$k_{23} = 0.1 – 4 \times 10^{-5}$
24	SOA + OH → SOA’	$k_{24} = 0.3 – 2.0 \times 10^{-12}$
25	BMPO-OH + OH → Product	$k_{25} = 0.1 – 5.0 \times 10^{-13}$

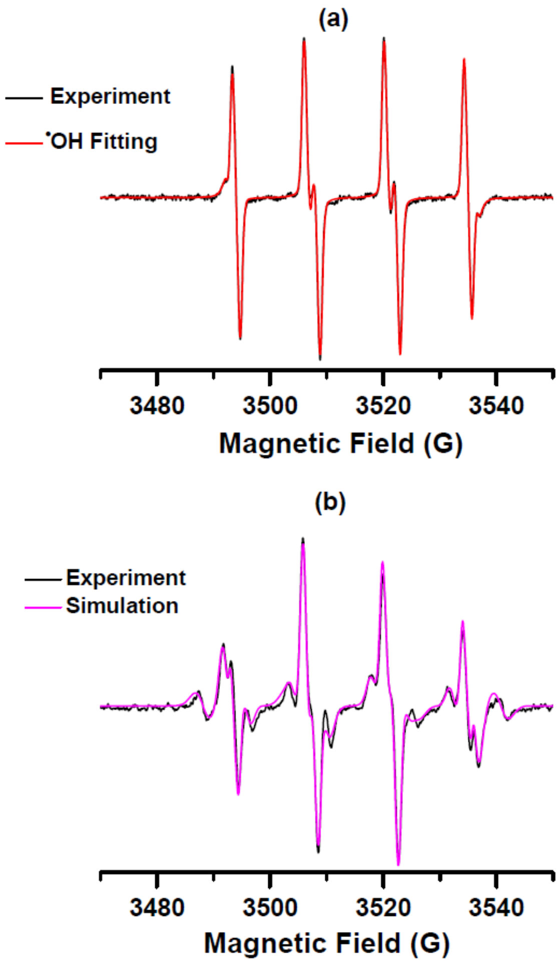

Figure S1. Measured, fitted and simulated EPR spectra. (a) Measured (black) and fitted (red) EPR spectra of water extracts of β-pinene SOA mixed with BMPO. (b) Measured (black) and simulated (pink) EPR spectra of a solution of tert-Butyl hydroperoxide mixed with BMPO.

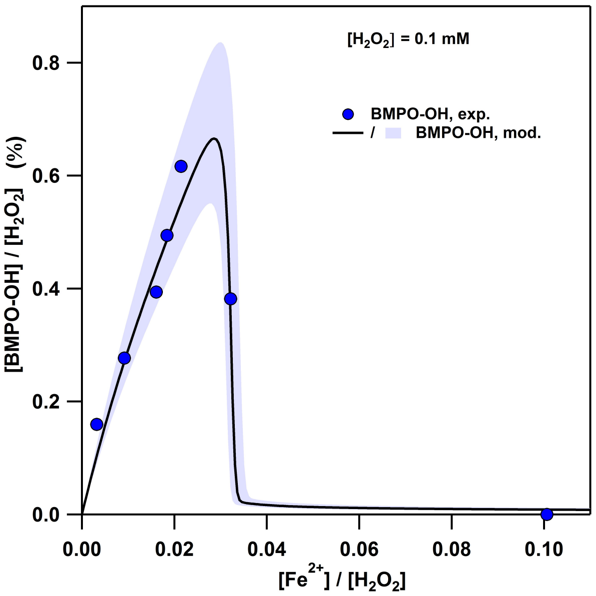

Figure S2. OH formation efficiency in H_2O_2/Fe^{2+} solutions. The concentrations of H_2O_2 and BMPO were 0.1 mM and 10 mM, respectively. The solid curve with shaded area is modelled with uncertainty.

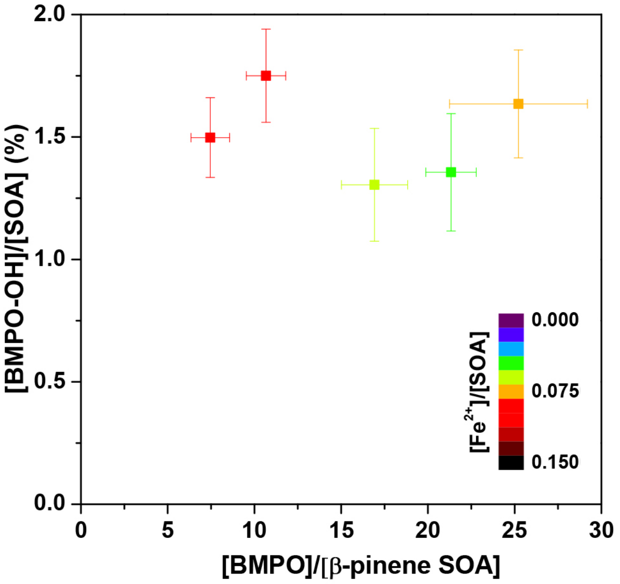

Figure S3. OH formation efficiency of β-pinene SOA/Fe^{2+} solutions as a function of BMPO concentration. The markers are colour coded with the molar ration of Fe^{2+} to SOA ([BMPO-OH]/[β-pinene SOA]).

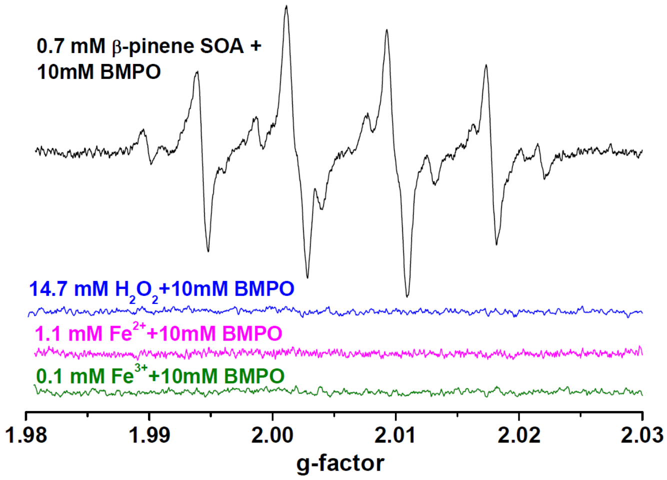

Figure S4. EPR spectra of BMPO mixtures. BMPO adducts with a 0.7 mM β-pinene SOA extracts (black line). Blank spectra of BMPO mixed with 14.7 mM H_2O_2 (blue line), 1.1 mM Fe^{2+} (pink line), and 0.1 mM Fe^{3+} (olive line) solutions. The BMPO concentration is 10 mM for all the samples.

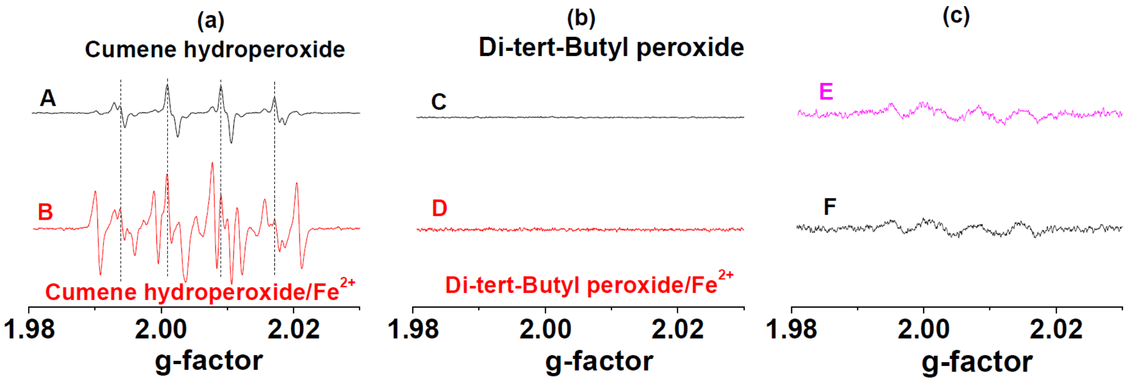

Figure S5. EPR spectra of various samples. EPR spectra of 15 mM cumene hydroperoxide solution in the absence of Fe^{2+} (A) and in the presence of 1.5 mM Fe^{2+} (B). EPR spectra of 15 mM Di-tert-Butyl peroxide solution in the absence of Fe^{2+} (C) and in the presence of 1.5 mM Fe^{2+}. EPR spectra of β-pinene SOA (E) and tert-Butyl hydroperoxide (F) in ethanol.

Supplementary references.

Bataineh, H., Pestovsky, O., and Bakac, A.: pH-induced mechanistic changeover from hydroxyl radicals to iron (IV) in the Fenton reaction, Chem. Sci., 3, 1594-1599, 2012.

Chevallier., E.: “Fenton-like” reactions of methylhydroperoxide and ethylhydroperoxide with Fe2+ in liquid aerosols under tropospheric conditions, Atmos. Environ., 38, 921, 2004.

Choe, E., and Min, D. B.: Chemistry and reactions of reactive oxygen species in foods, J. Food. Sci., 70, R142-R159, 2005.

Christensen, H., Sehested, K., and Corfitzen, H.: Reactions of hydroxyl radicals with hydrogen peroxide at ambient and elevated temperatures, J. Phys. Chem., 86, 1588-1590, 1982.

Corradi, M., Pignatti, P., Brunetti, G., Goldoni, M., Caglieri, A., Nava, S., Moscato, G., and Balbi, B.: Comparison between exhaled and bronchoalveolar lavage levels of hydrogen peroxide in patients with diffuse interstitial lung diseases, Acta Biomed, 79, 73-78, 2008.

Deguillaume, L., Leriche, M., Desboeufs, K., Mailhot, G., George, C., and Chaumerliac, N.: Transition Metals in Atmospheric Liquid Phases: Sources, Reactivity, and Sensitive Parameters, Chem. Rev., 105, 3388-3431, 2005.

Divišek, J., and Kastening, B.: Electrochemical generation and reactivity of the superoxide ion in aqueous solutions, J. Electroanal. Chem., 65, 603-621, 1975.

Ghio, A. J., Turi, J. L., Yang, F., Garrick, L. M., and Garrick, M. D.: Iron homeostasis in the lung, Biol. Res., 39, 67-77, 2006.

Ghio, A. J.: Disruption of iron homeostasis and lung disease, Biochimica et Biophysica Acta (BBA) - General Subjects, 1790, 731-739, 2009.

Guo, Q., Qian, S. Y., and Mason, R. P.: Separation and identification of DMPO adducts of oxygen-centered radicals formed from organic hydroperoxides by HPLC-ESR, ESI-MS and MS/MS, J. Am. Soc. Mass Spectrom., 14, 862-871, 2003.

Herrmann, H., Schaefer, T., Tilgner, A., Styler, S. A., Weller, C., Teich, M., and Otto, T.: Tropospheric Aqueous-Phase Chemistry: Kinetics, Mechanisms, and Its Coupling to a Changing Gas Phase, Chem. Rev., 115, 4259-4334, 2015.

Hunter, R. C., Asfour, F., Dingemans, J., Osuna, B. L., Samad, T., Malfroot, A., Cornelis, P., and Newman, D. K.: Ferrous iron is a significant component of bioavailable iron in cystic fibrosis airways, MBio, 4, e00557-00513, 2013.

Koppenol, W. H., Butler, J., and Leeuwen, J. W. v.: The Haber ‐ Weiss cycle, Photochem. Photobiol., 28, 655-658, 1978.

Paget-Brown, A. O., Ngaintrakulpanit, L., Smith, A., Bunyan, D., Hom, S., Nguyen, A., and Hunt, J. F.: Normative data for pH of exhaled breath condensate, Chest, 129, 426-430, 2006.

Rush, J. D., and Bielski, B. H. J.: Pulse radiolytic studies of the reaction of perhydroxyl/superoxide O_2^- with iron(II)/iron(III) ions. The reactivity of HO_2/O_2^- with ferric ions and its implication on the occurrence of the Haber-Weiss reaction, J. Phys. Chem., 89, 5062-5066, 1985.

Sarangapani, R., and Wexler, A. S.: The role of dispersion in particle deposition in human airways, Toxicol. Sci., 54, 229-236, 2000.

Sehested, K., Rasmussen, O. L., and Fricke, H.: Rate constants of OH with HO_2,O_2^-, and $H_2O_2^+$ from hydrogen peroxide formation in pulse-irradiated oxygenated water, J. Phys. Chem., 72, 626-631, 1968.

Stuglik, Z., and PawełZagórski, Z.: Pulse radiolysis of neutral iron (II) solutions: oxidation of ferrous ions by OH radicals, Radiat. Phys. Chem., 17, 229-233, 1981.

Walters, D. V.: Lung lining liquid–The hidden depths, Neonatology, 81, 2-5, 2002.